World Academy of Science, Engineering and Technology
International Journal of Architectural and Environmental Engineering
Vol:12, No:2, 2018

Numerical Simulation of Lightning Strike Direct Effects on Aircraft Skin Composite Laminate

Muhammad Khalil, Nader Abuelfoutouh, Gasser Abdelal, Adrian Murphy

***Abstract*—**Nowadays, the direct effects of lightning to aircrafts are of great importance because of the massive use of composite materials. In comparison with metallic materials, composites present several weaknesses for lightning strike direct effects. Especially, their low electrical and thermal conductivities lead to severe lightning strike damage. The lightning strike direct effects are burning, heating, magnetic force, sparking and arcing. As the problem is complex, we investigated it gradually. A magnetohydrodynamics (MHD) model is developed to simulate the lightning strikes in order to estimate the damages on the composite materials. Then, a coupled thermal-electrical finite element analysis is used to study the interaction between the lightning arc and the composite laminate and to investigate the material degradation.

***Keywords*—**Composite structures, lightning multiphysics, magnetohydrodynamics, coupled thermal-electrical analysis, thermal plasmas.

I. Introduction

LIGHTNING strike is a particularly important aspect of aircraft skin design. They represent a severe threat that has to be given serious consideration by international aeronautical industries because lightning can cause major damage, in particular, to composite ones. Lightning-aircraft interaction, and more precisely, lightning-composite interaction is difficult to apprehend due to the lack of complete studies in this domain. Some authors have focused on the observed damage following a lightning strike. These visible damages mainly occur at the "surface" and correspond mainly to removal of paint and metal protection but may also extend to the first CFRP plies [5], [8], others have presented a coupled electromagnetic/thermal Finite Element (FE) model to simulate lightning strikes numerically. Their model coupled electromagnetic and thermal behaviour for specimens without lightning strike protections to compute the temperature flux in the material. They assumed that the electrical conductivity evolved linearly with the temperature varying with matrix decomposition to carbon sublimation [3]. Some other works [9] studied the interaction between the lightning arc and various aeronautic skins, including composite and aluminium ones. They worked on various skins' conductivity due to Joule heating, Laplace forces and resistive heating, to study the influence of material's skin conductivity on the observed damage mechanisms and arc root spreading at the surface. Finally, in their study, Abdelal and Murphy [4] also worked on a coupled electro-thermal model but this time taking into account the formulation of temperature dependent material properties, using FE method to model the composite material and the embedded ECF protection.

In order to standardize its representation, an international current density profile versus time has been defined [1], [2]. This profile is composed of four parts: two pulse parts and two quasi continuous ones, which are used by aircraft manufacturers to represent and to test the material impacted by lightning. This paper presents our contribution to this area by the development of a calculation code. For this study, we are not interested in the total current density variation but only in the continuous part, C, which can be legitimately modelled by a free-burning arc of a few hundred amperes according to Larsson et al. [15], [16] and Uhlig [17]. First, 2D MHD models were carried out, and energy fluxes were transferred to the anode under study. The commercial code COMSOL Multiphysics, version 5.0, was used to represent the free-burning arc configuration in an air plasma impacting the composite anode. Then, a three-dimensional (3D) model is thus developed and used to evaluate the degradation of the composite material under lightning strike effects. The mathematical calculations show the importance of taking into account the Joule effect term in the material, in this kind of configuration.

II. Lightning and Aircraft

A. Aircraft Zoning

The various parts of an aircraft are not homogeneously exposed to equivalent risks. In order to protect aircrafts from lightning strikes, studies have been led to establish a map of the structure, which sheds light on the zones where lightning is often attached. An aircraft is thus chopped in zones exposed to part of the threat described by the preceding wave of current. The definition of these zones also constitutes a mandatory certification step of the international regulations [1], [2] (EUROCAE and SAE). It allows engineers to predict the "danger zones" and to protect the structure adequately. These studies end up to what is called the zoning which divides the aircraft into sections typically impacted by one or another component of the lightning presented in Fig. 1.

Three zones of interest are exposed:

Zone 1. (A and B) corresponds to the parts of high probability of initial lightning flash attachment (entry or exit).

Zone 2. (A and B) corresponds to the parts of high probability of a lightning flash being swept from a point of initial attachment.

Muhammad Khalil and Nader Abuelfoutouh are with the Aerospace Engineering Department, Cairo University, 12613 Giza, Egypt (e-mail: Muhammad.hamza@eng1.cu.edu.eg, naderabuelfoutouh@eng.cu.edu.eg).

Gasser Abdelal and Adrian Murphy are with the School of Mechanical and Aerospace Engineering, Queen's University, BT7 1NN Belfast, UK (e-mail: g.abdelal@qub.ac.uk, a.murphy@qub.ac.uk).

Zone 3. corresponds to the other parts of the aircraft. Any aircraft surface other than those covered by zones 1 and 2. In zone 3 there is a low probability of a direct attachment, however, zone 3 areas may carry substantial lightning currents by direct conduction between two attachment points.

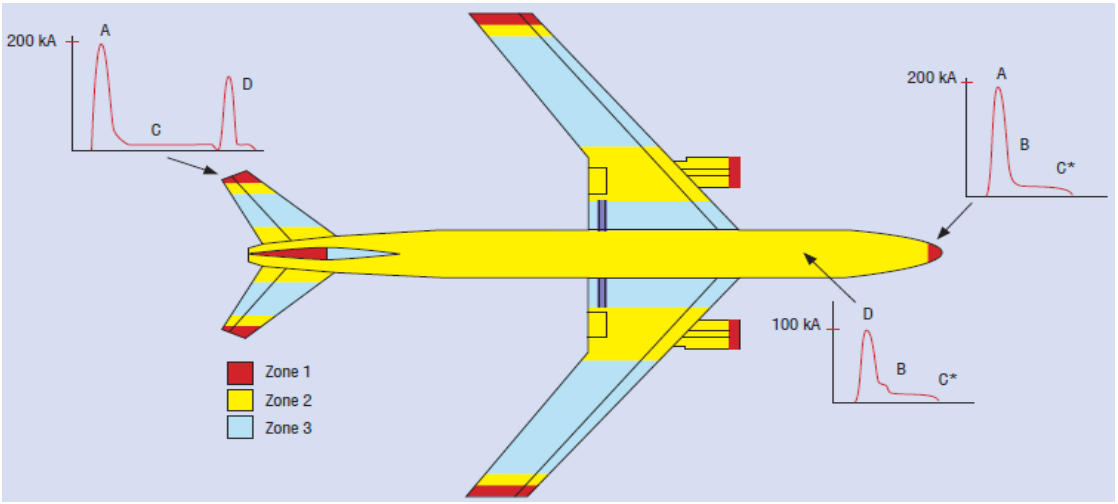

Fig. 1 Aircraft Zoning [1], [2]

The study of lightning strike sheds light on two major effects that they caused on composite structures: direct and indirect effects. This paper will be mainly focused on the direct effects induced by lightning to composite panels that constitute the structure of aircrafts, in particular, for those which relate to the Joule effect and the dissipation of the energy by conduction.

B. Indirect Effects of Lightning

Lightning current induces effects in wiring and equipment by electromagnetic coupling (induction, and aggression by electric and magnetic fields).

C. Direct Effects of Lightning

The direct effects of lightning on an aircraft are the physical damage suffered by the aircraft due to the direct attachment of the arc channel and the conduction of the lightning current inside the aircraft structure.

III. The International Regulation & Laboratory Tests

The first version of the international regulation goes back to 1972 and was established by the SAE (Society of Automotive Engineers) in order to study and certificate aircraft against the lightning threat, aircraft manufacturers have to define this threat and define proper laboratory means that would allow them to reproduce it. Conjoint works by the NASA, FAA and industry have led to a recommended procedure when it comes to lightning: the SAE ARP 5412. This report is internationally considered as the sole standard concerning the lightning threat [2]. This threat is defined using data of lightning to the ground [1]. This threat is defined using data from ground strikes. Indeed, it is only in this configuration where significant statistical data exist. The results obtained at the time of the trial runs in flight suggest that the lightning threat in flight is less than that on the ground.

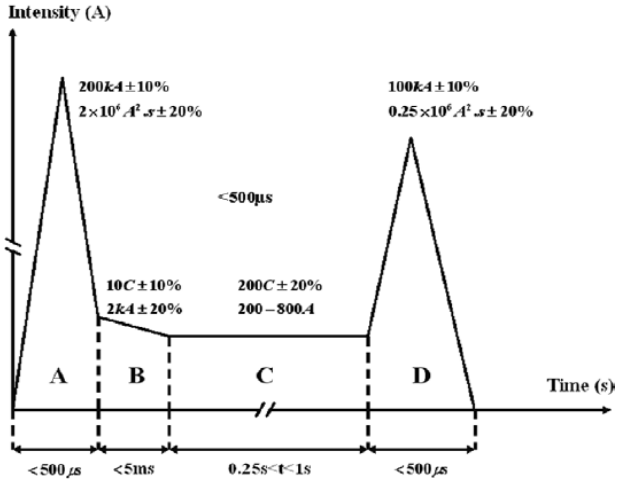

Fig. 2 Normalized current for lightning strike tests in laboratory [6]

In the current standard, the natural lightning environment is represented by components A, B, C and D (Fig. 2). The wave thus defined covers 99% of the strikes on the ground in severity. The various parameters making it possible to define this wave are the following:

- The intensity peak of the current.
- The rise and descent times of the wave front.
- The electrical load transferred equals to $\int$ idt (in C).
- The action integral equals to $\int i^2dt$ (in $A^2.s$ or J/Ω) that represents the ability of the current to deposit energy on a resistive object.

Component A. Current of the first return stroke: this component has a peak intensity of 200 kA±10%, an action integral of 2×10^6 $A^2.s$ ± 20% and a total duration of 500 µs at the maximum. The rise time from 10% to 90% of the peak

value must be smaller than 50 µs (compared to the component D). This component can cause damage by direct effects or indirect effects.

Component B. intermediate current: this component has an average amplitude of 2 kA ± 20% and an electrical load transferred of 10 C±10% during 5 ms ± 10%. This component corresponds to a transition phase of the discharge.

Component C. continuous current: This component transfers an electrical load of 200 C±20% during a time between 0.25 and 1 second, with intensity from 200 to 800 A. This component of limited amplitude can cause very important damages (in particular thermal ones) because of large quantity of electrical charges that it deposits.

Component D. current of the subsequent return stroke: this component has a peak intensity of 100kA ± 10%, an action integral of 0.25 $\times 10^6$ A^2.s ± 20% and a total duration of 500µs at the maximum. The time from 10% to 90% of the peak value must be smaller than 25 µs.

This evolution is used by aircraft manufacturers in the testing and certification of materials used on planes. In this paper, we will study only the continuous part C, which leads to the greatest composite degradation, and which can be simulated, according to several authors, by a free burning arc of several hundred amperes [15], [16].

IV. 2D MHD Model

For this study, a lightning arc can be assimilated as a free electrical arc during the continuous phase of current wave. Consequently, a MHD approach is used. It consists of coupling of the Navier-Stokes equations, which estimate the fluid flow characteristics and the heat transfer equations, which estimate the temperature profile with the Maxwell equations, which estimate the electromagnetic aspects of the arc. The interaction between the lightning arc and an electrode representing the composite laminate is studied to quantify the various transfers of energy between plasma and materials versus the pulse duration and the current intensity value. This model shows the behaviour of the plasma column representing the lightning strike and quantifies the power transferred to the anode. The governing equations with 2D axi-symmetric of the numerical model are solved by using a commercial code (COMSOL Multiphysics version 5.0) based on the FE method. The code was adapted to take into account the "electromagnetic aspects" and the interactions between the electrical arc and the anode. A comparison with experimental results is presented. So, an axisymmetrical configuration with a two-dimensional coordinate system (r, z) is used in a transitory state.

A. Assumptions

To simplify the problem, the following assumptions are considered: The arc is stationary; therefore we use an axisymmetric coordinate system, the plasma is a single incompressible Newtonian fluid and is assumed to be air at Local Thermodynamic Equilibrium (LTE), the convection generated by the Lorentz forces can be treated as a laminar flow, the gravity effects are neglected and the anode surface is assumed to be flat over time, the radiation from the plasma to the anode and reciprocally is neglected, and atmospheric pressure is assumed.

Based on the above assumptions, the classical Navier-Stokes equations for a Newtonian viscous fluid must be considered to get the velocity, pressure, and temperature fields.

1. Electric Module (ec) & Magnetic Module (mf)

The electromagnetic behaviour is modelled using the classical Maxwell's equations computed in the cathode, arc-plasma and anode, (1)-(6),

$$\nabla x \vec{H} = \sigma \vec{E} + \varepsilon \frac{\partial \vec{E}}{\partial t} \tag{1}$$

$$\nabla x \vec{E} = -\mu \frac{\partial \vec{H}}{\partial t} \tag{2}$$

$$\vec{B} = \mu_0 \vec{H}, \vec{D} = \varepsilon \vec{E} \tag{3}$$

$$\vec{E} = -\nabla V - \frac{\partial \vec{A}}{\partial t} \tag{4}$$

$$\vec{J} = \sigma\left(\vec{E} + \vec{v} x \vec{B}\right) + \frac{\partial \vec{D}}{\partial t} \tag{5}$$

$$\sigma \frac{\partial \vec{A}}{\partial t} + \nabla x \left(\frac{1}{\mu} \nabla x \vec{A}\right) + \sigma \nabla V = -\nabla V - \frac{\partial \vec{A}}{\partial t} \tag{6}$$

where $\vec{H}$ is the vector magnetic field intensity, $\vec{D}$ is the electric displacement vector, σ is the electrical conductivity of the corresponding domain (cathode, plasma, anode), $\vec{J}$ is the current density, ε is the dielectric constant (permittivity), μ_0 is the domain permeability, $\vec{E}$ is the electrical field intensity, V is the electrical potential, $\vec{B}$ is the magnetic flux density, and $\vec{A}$ is the magnetic potential. But, in these expressions, the temporal term $\partial \vec{A}/\partial t$ has a little variation in the plasma column due to the small temporal variation of the current density components. They will be neglected for the rest of the study.

2. Fluid Flow Equations (spf)

The fluid flow in the whole domain is described by the classical conservation equations. Based on the assumptions above, the conservations equations can be expressed in a time-dependent form as follows:

Conservation of mass

$$\frac{\partial \rho}{\partial t} + \nabla . (\rho \vec{v}) = 0 \tag{7}$$

Conservation of momentum

$$\rho\left(\frac{\partial \vec{v}}{\partial t} + \vec{v} . \nabla \vec{v}\right) = \nabla . \left[-pI + \mu(\nabla \vec{v} + (\nabla \vec{v})^T) - \frac{2}{3}\mu(\nabla . \vec{v})I\right] + \vec{J} \times \vec{B} \tag{8}$$

where $\vec{v}$ is the velocity vector field, t is time, ρ is density, μ is viscosity, p is the pressure field, $\vec{J}$ is electric current density,

and $\vec{B}$ is the magnetic flux density.

3. Heat Transfer Module (ht)

The energy conservation equation is used to model heat transfer in the fluid and solid domains, (9),

Conservation of Energy

$$\rho C_p \left[\frac{\partial T}{\partial t} + \vec{v}.\nabla T\right] = \nabla.(k\nabla T) + \vec{J}.\vec{E} + \frac{5k_B}{2e}\vec{J}.\nabla T - 4\pi\varepsilon_N \quad (9)$$

The last three terms in the above equation are; the joule heating effect, the electronic enthalpic flux (the energy contribution of the electrons due to the increase of their kinetic energy in the plasma column), and the plasma radiation loss respectively. Where T is the temperature, k is the thermal conductivity, k_B is the Boltzmann constant, e is the electron charge, and ε_N is the net emission coefficient of plasma, that varies with temperature [11]. In addition, the ohmic sheath zone permeability is very low (1 x 10^{-15}). The thermodynamic and transport properties are from [10] and from the thesis of Naghizadeh for the net emission coefficient [11].

Physically, between the plasma column and the two electrodes a thin layer exits which is not in LTE. In fact, the heavy particles temperature is close to the electrodes materials temperature (2000-3500 K), whereas the electron temperature is much higher in order to ensure the current conduction between the plasma and the electrodes [17]. Thus, a solution assuming LTE in the whole plasma domain is impossible for a finite current. To take into account all the non-LTE effects near the electrodes, one must develop a twin temperature model: electron temperature and ions temperature. However, there are methods that permit numerically to ensure the electrons conduction between the arc-plasma and the electrodes: Thus, the temperature boundary condition at the cathode (3500 K) is assumed by many researchers to resolve the issue of zero electric conductivity at room temperature [12].

B. Computational Domain and Boundary Conditions

A sketch of this process is shown in Fig. 2. Arc plasma between two electrodes: the anode (+) which represents the workpiece and the cathode (-) which represents the source of electrons.

The calculation domain used in this study is shown in Fig. 3. The geometry includes a tungsten cathode with a 35° angle tip and 20 mm length. The cathode tip is flattened. The anode has a thickness of 4 mm and a radius of 20 mm. The inter electrode distance, that is to say the arc length, is typically 3 mm.

Table I defines the material properties for all domains; while Table II defines the applied classical boundary conditions for a free burning arc configuration are used. The model consists of three basic domains, cathode, anode and fluid (air plasma). The anode in this simulation is the aircraft composite laminate. Air plasma's transport properties are taken from references [10], while assuming the air plasma is in local thermodynamic equilibrium (LTE).

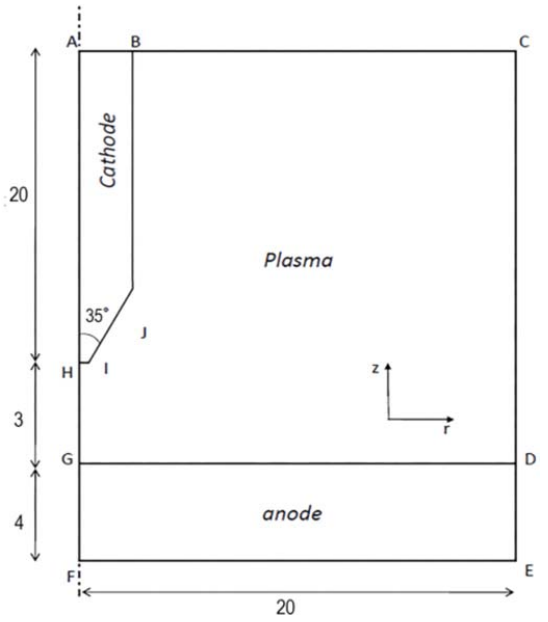

Fig. 3 Computational domains, dimensions are in mm

Material properties for the anode and the cathode domains are defined as a function of temperature (COMSOL Material Library). The thermodynamic and the transport properties depend on the local temperature and on the nature of the medium. Zero initial conditions are assumed for all domains.

Table II lists all the boundary conditions of the unified problem. The most pertinent points are outlined below:

Regarding the thermal conditions, the temperature along the external boundaries ABC and CD is set to the ambient temperature $T_0 = 300$ K, one must be careful to take a long enough cathode length in order to be sure that the temperature along the previous boundaries is close to the ambient temperature.

TABLE I
MATERIAL PROPERTIES FOR ALL DOMAINS

Air Gas Plasma Properties. Air ionization potential = 12.1 V. The thermodynamic and transport properties are from [10] and from the thesis of Naghizadeh [11] for the net emission coefficient. Cathode work function = 4.52 V, effective work function = 2.63 V, Richardson's constant = 3 x 10^4 A m^{-2} K^{-2} [14]. Anode: Copper. COMSOL Material Library. Cathode: Tungsten [solid]. COMSOL Material Library.

TABLE II
MODEL BOUNDARY CONDITIONS

	AB	*BC*	*CD*	*DE*	*EF*
T	$T = 300K$	$T = 300K$	$T = 300K$	$T = 300K$	$T = 300K$
(u,v,p)	–	$p = p_o$	$p = p_o$	$\vec{v} = \vec{0}$	$\vec{v} = \vec{0}$
$(V,\vec{A})$	–	$\vec{j}.\vec{n} = \vec{0}$	$\vec{j}.\vec{n} = \vec{0}$	$\vec{j}.\vec{n} = \vec{0}$	$V = 0$
		$\vec{A}.\vec{n} = \vec{0}$	$\vec{A}.\vec{n} = \vec{0}$	$\vec{A}.\vec{n} = \vec{0}$	
	FH	*HA*	*HB*	*GD*	
T	$\vec{q}.\vec{n} = \vec{0}$	$\vec{q}.\vec{n} = \vec{0}$	$T = 3500K$	(10)	
(u,v,p)	$\vec{v}.\vec{n} = \vec{0}$	–	(11)	$\vec{v}.\vec{n} = \vec{0}$	
$(V,\vec{A})$	$V = 0$	$\vec{j}.\vec{n} = \vec{0}$	$\vec{v} = \vec{0}$	$[\![\vec{j}.\vec{n} = \vec{0}]\!]$	
		$\vec{B}.\vec{n} = \vec{0}$	$[\![\vec{j}.\vec{n} = \vec{0}]\!]$		

C. The Heat Transfer at the Arc-Electrodes Interfaces

The Arc/Anode Interface

$$q_{anode}.\vec{n} - \vec{q}_{pl}.\vec{n} = |\vec{J}.\vec{n}|\emptyset_a - \varepsilon k_B T^4 \quad (10)$$

where $q_a = -k_a \nabla T_a$, $q_{pl} = -k_{pl} \nabla T_{pl}$, k_a is the anode thermal conductivity, k_{pl} is the plasma thermal conductivity, T_a and T_{pl} represent the temperature field respectively in the anode and plasma domains. $\vec{n}$ is a vector normal to the electrodes surfaces and directed toward the plasma domain as shown in Fig. 4, $\emptyset_a$ is the work function of the anode, ε is the anode emissivity, and k_B the Boltzmann's constant.

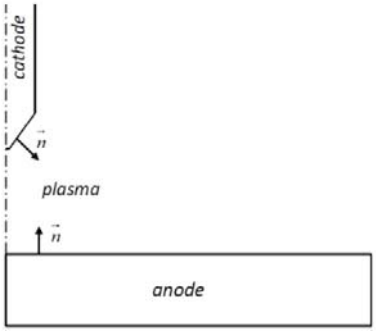

Fig. 4 Definition of the normal vector to the electrodes surfaces

The first term $|J.n|\emptyset_a$ represents the heating by electron condensation (energy received by the anode from the incoming electrons). The second term $\varepsilon k_B T^4$ represents the radiation cooling losses. The heat flux at the boundary between the cathode and the plasma has to satisfy (11) [12].

The Arc/Cathode Interface

Similarly to the anode region, the following energy balance is considered at the interface between the arc-plasma and the cathode:

$$q_{cathode}.\vec{n} - q_{pl}.\vec{n} = j_i V_i - j_e \emptyset_c - \varepsilon k_B T^4 \quad (11)$$

where $q_c = -k_c \nabla T_c$, k_c is the cathode thermal conductivity, k_{pl} is the plasma thermal conductivity, T_c and T_{pl} represent the temperature field respectively in the cathode and plasma domains, j_i and j_e are respectively the ion current and the electron current, $\emptyset_c$ is the cathode work function, and V_i is the air ionization potential. The first term $j_i V_i$ represents the heating energy received by the cathode from the impacted ions. The second term $j_e \emptyset_c$ represents the energy consumed at the cathode to emit electrons. The electron and ion currents are calculated from (12) [14], a method developed by Lowke et al. [13];

$$J_r = A_r T^2 exp\left(-\frac{e\emptyset_e}{k_B T}\right) \quad (12)$$

$$j_e = \begin{cases} j_r \; if \; (|\vec{j}.\vec{n}| - j_r) > 0 \\ |\vec{j}.\vec{n}| \; if \; (|\vec{j}.\vec{n}| - j_r) \leq 0 \end{cases}$$

$$j_i = |\vec{j}.\vec{n}| - j_e$$

where A_r is the Richardson's constant, $\emptyset_e$ is the effective work function for thermionic emission, e is the elementary charge, and k_B is the Boltzmann's constant. The electron current density j_e cannot exceed the Richardson current density j_r.

1. Waveform-C Simulation

Indeed, this is a chopped voltage waveform in which breakdown of the gap between an object under test and the test electrodes occurs at 2 μs (±50%). The amplitude of the voltage at time of breakdown and the rate-of-rise of voltage prior to breakdown are not specified. A typical pulsed current signal applied on cathode in Fig. 5. For this study, the current density varies from 400 A for an arc life duration from 0 to 0.5 s in order to ensure that the electric charge deposited on the anode material is 200 C (±20%). This waveform should be unidirectional; e.g. rectangular, exponential or linearly decaying.

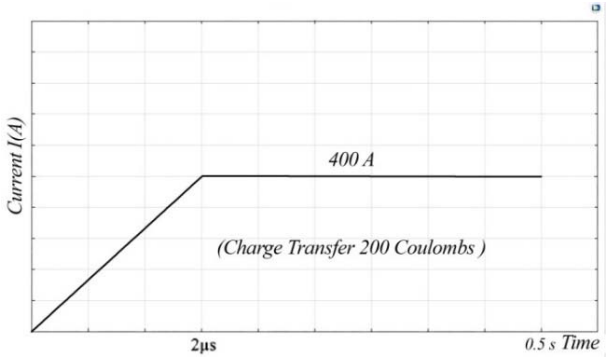

Fig. 5 A typical pulsed current used in the model

2. *FE* Model

All the above equations of the problem are solved using the FE method. The calculation flowchart is shown in Fig. 6.

After a time step, the electric and magnetic potentials are first computed. Then, the current density, electric field, and magnetic induction are deduced in the whole domain. The computed Joule heat source is then used to calculate the temperature field. Pressure and velocity are obtained using the previously computed thermal field and the Lorentz force. If the convergence criteria are not reached, the thermo-physical properties are updated using the current temperature and calculations will continue until convergence. Finally, the whole process is repeated at each time step until the end of time.

To model this configuration, we use a grid of a sequence type, physics -controlled mesh with element size which is an extremely fine. Complete mesh consists of 30233 domain elements and 689 boundary elements as shown in Fig. 7.

3. Results and Discussion

In the present section, the results of the model are obtained for the free-burning arc configuration. It should be noted that the model has already been validated in terms of plasma

temperature fields (comparison with [18]), and in terms of heat flux and current density profile at the anode surface (comparison with [19]). The results for our current density case [400A], in terms of temperature field and in terms of flux density injected in the anode, are represented in the following figures.

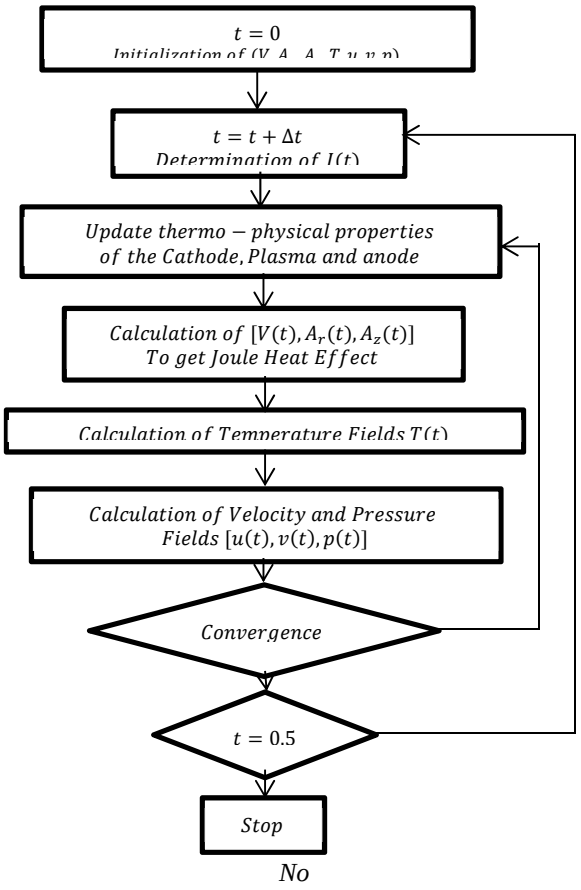

Fig. 6 Flowchart of lightning MHD model multiphysics calculations

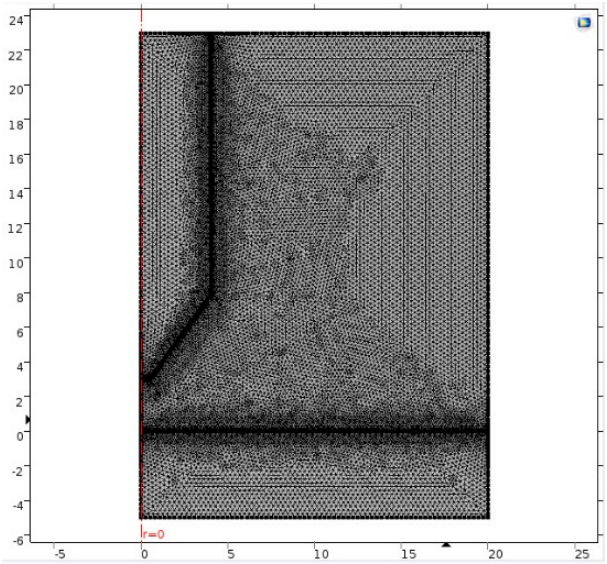

Fig. 7 FE mesh domain

D.Experimental Validation

The results reported in [18] do not permit further validation of the developments presented here. The Nestor experiment [19] is used to validate the current density profiles at the anode surface (segment GD in Fig. 3). The result is identical to our model except for the inter-electrode distance (6.3 mm instead of 3 mm). The current density and total flux injected at the surface of the anode is practically the same between the Nestor experiment and the proposed model (Figs. 8 and 9).

The results are the same order of magnitude. The difference could be explained by the fact that in Hsu's model [18] the electrodes were not taken into account in the resolution domain and were considered like boundary conditions. Moreover, the meshing is different between the two models and, in [12]; it is proved that cathode angles influence the position and the value of the maximum velocity of plasma on the axis.

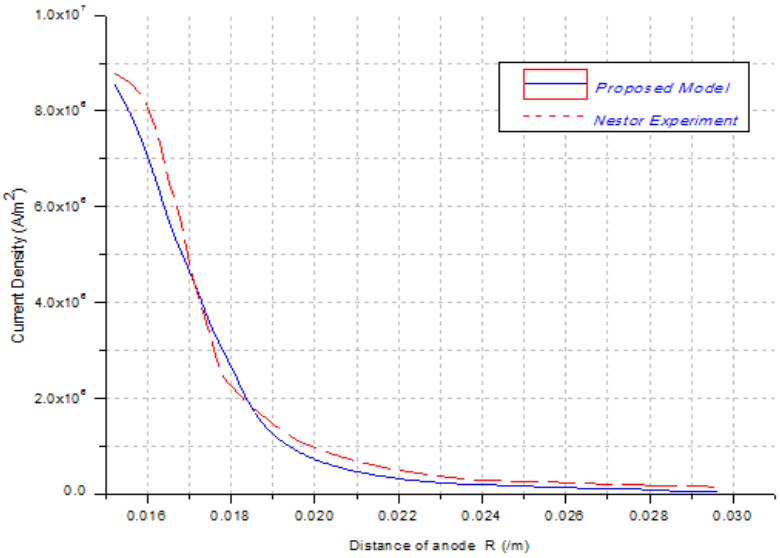

Fig. 8 Current density injected at the surface of the anode

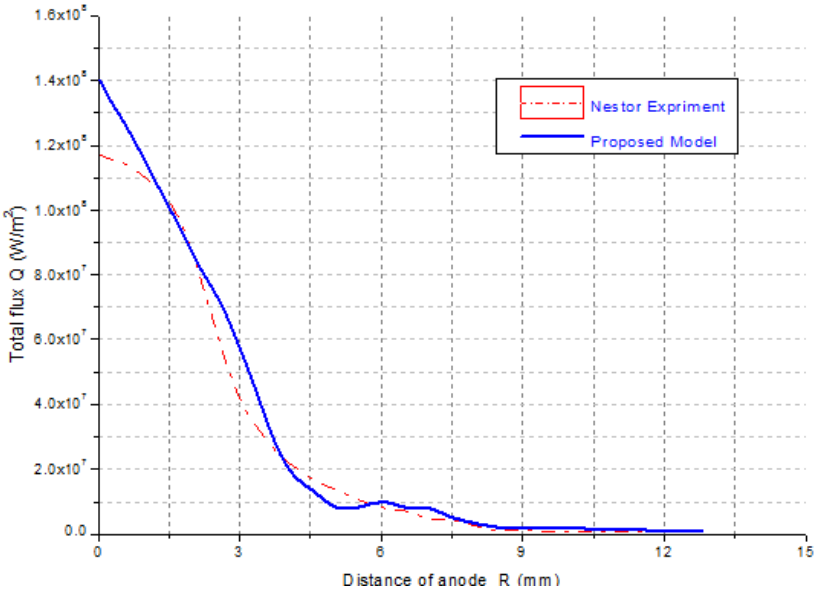

Fig. 9 Total flux injected at the surface of the anode

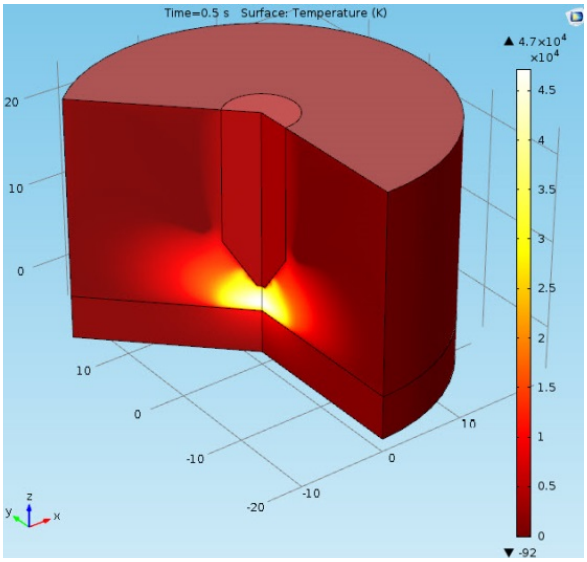

Fig. 10 3D- Revolution for temperature profile waveform-C at time = 0.5 s

The results in terms of temperature field (of the order of 40,000 K), or more exactly, in terms of material degradation, are represented in Figs. 10 and 11 at t = 0.5 s.

It is notice that once the plasma reaches the anode surface and due to air electric resistivity, the channel starts to heat up and expand. Expansion of the plasma channel leads to a wider anode surface area that is exposed to electric current and the average electric current density is reduced (Fig. 11).

The results in terms of velocity field are represented in Figs. 12 and 13 at t = 0.5 s. To verify the accuracy of the free-burning arc model, some comparisons have been made.

Figs. 11 and 12 present the temperature and velocity of plasma on the axial (400A air plasma); the maximum values are respectively 45,900 K and 333 m/s, which are close to the numerical results of Hsu [18].

Figs. 8 and 9 present the current density and total flux on the anode surface (400A air plasma). The maximum values are respectively 8.66×10^{6} A·m^{-2} and 1.45×10^{8} W·m^{-2}, which are close to the values obtained in the previous work. However, some noticeable differences exist, which might be the result of different thermal and electrical conductivities of the anode surface.

Fig. 11 shows the temperature distribution of the air plasma. The temperature reaches a maximum of 40,000 K. With an increase in the distance of the cathode, the temperature decreases owing to the entrained air and the anode provides a cooling effect.

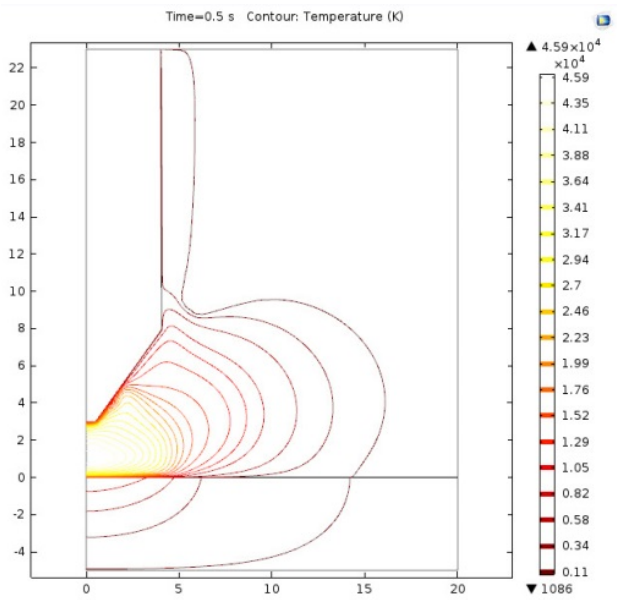

Fig. 11 Isotherms of waveform-C at time = 0.5 s

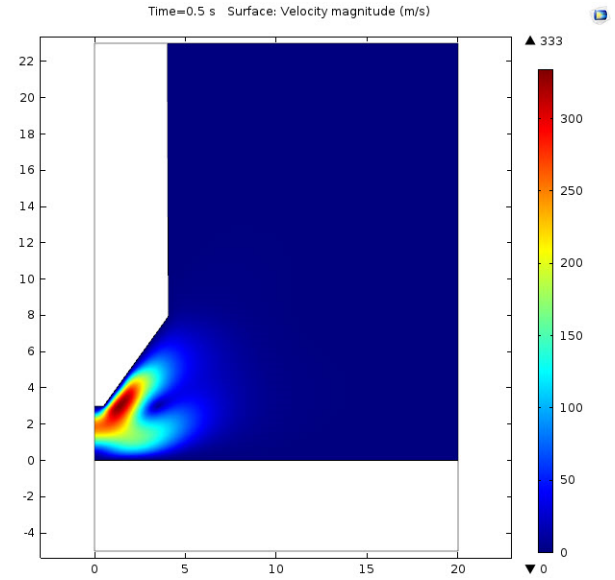

Fig. 12 Velocity profile waveform-C at time = 0.5 s

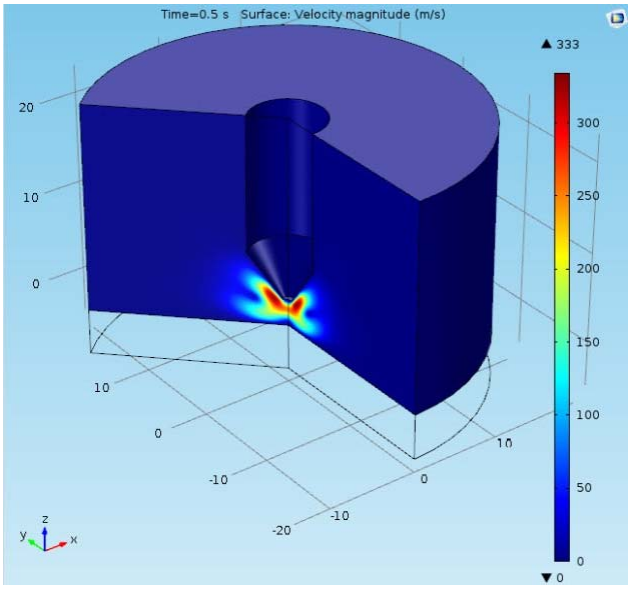

Fig. 13 3D- Revolution velocity profile waveform-C at time = 0.5 s

The pressure loading (of the order of 0.1-0.2 MPa) during a Waveform-C event will have a minimal effect on composite material damage (Fig. 14).

V. Interaction with the Composite Laminate

This study presents the numerical procedure to investigate the impact of lightning strike on composite panel which is decomposition of the laminates in the area of the lightning strike, and delamination of the laminates near the impact area due to decomposition and far from the impact area due to the progression of the thermal stress shock. Using experimental tests to study the impact of lighting strike is expensive and limited to studying the effect of few parameters, such as decomposition and delamination in the vicinity of the lighting strike. Yet it fails to study laminates delamination far from the impact area and becomes more expensive to optimize the lightning protection systems performance or to study the stochastic of the process. We had investigated the current density and total heat flux that conduct from the plasma arc the aircraft surface. Thus, a 3D model is thus developed and used to evaluate the degradation of the composite material under lightning strike effects. A coupled thermal-electrical FE analysis is used to investigate the design variables that can affect lightning strike damage on epoxy/graphite composite panels by using the commercial code (ABAQUS version 6.12.1). We used heatval user material subroutine to model the decomposition kinetics and heat. Damage in composite material can be reduced by increasing the value of decomposition heat. The contribution of this study is modeling the composite panels' material properties as temperature dependent, which was excluded by other researchers. A number of practical solutions to minimize the damage effect are proposed.

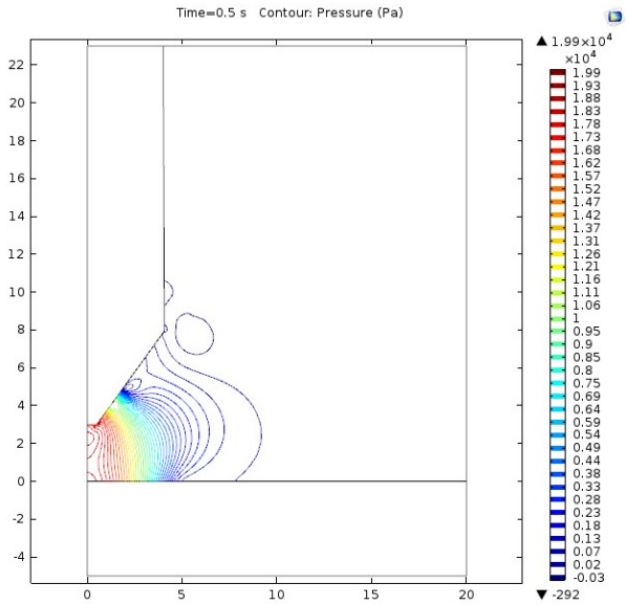

Fig. 14 Absolute pressure profile waveform-C at time = 0.5 s

A. FE Model

The composite panel is divided into two partitions. One partition represents the region under lighting strike conducting channel. A second partition represents the remaining part of the composite panel. Latent decomposition heat of composite is 4.8 x 10^3 kJ/kg, which is released between the temperature ranges of $[300^oC - 500^oC]$. Latent sublimation heat, which is released at sublimation temperature $[3316^oC]$ is 43 x10^3 kJ/kg.

Composite laminates are 32-ply quasi-isotropic ($[45^o/0^o/-45^o/90^o]_{4s}$). The thickness of each ply is 0.147 mm, resulting in the total thickness which is approximately 4.7 mm. A specimen has 300 mm width and 300 mm length. Each lamina of the composite laminate is meshed using an eight-node isoperimetric solid element to the plane of symmetry of the composite panel.

Orthotropic material properties calculated using a rule of

mixture are used for the elements that are meshing the bottom half of the composite panel. The thermal conductance between composite laminates was measured experimentally and its value at room temperature is $500W/m^2.K$. As the epoxy thermal conductivity is reduced by 30% after it is decomposed, the thermal conductance is also reduced by the same percentage. There is no available published data for the electric conductance and it is assumed perfect in this work.

The composite material is made of carbon fiber/epoxy (IM600/133). Material thermal/Electrical properties, such as thermal conductivity, specific heat, and sublimation heat are defined from [4].

B. Boundary Conditions

The boundary conditions are as follows in Fig. 15. The electrical potential at the bottom of a specimen is assumed to be zero, because a conducting copper plate under the bottom of a specimen was electrically grounded. The electrical potential at the side surfaces is assumed as zero, because the electrical discharge from the side surfaces to the bottom copper plate was observed during all of the impulse tests. Thermal radiation was given for the upper and side surfaces of a specimen, whereas the bottom surface was adiabatic. Although it was understood that the heat transfer to copper plate at the bottom surface should be examined, the temperature increment at the bottom was almost zero. It was therefore ignored. The emissivity and environment temperature were, respectively, 0.9 and 25^oC.

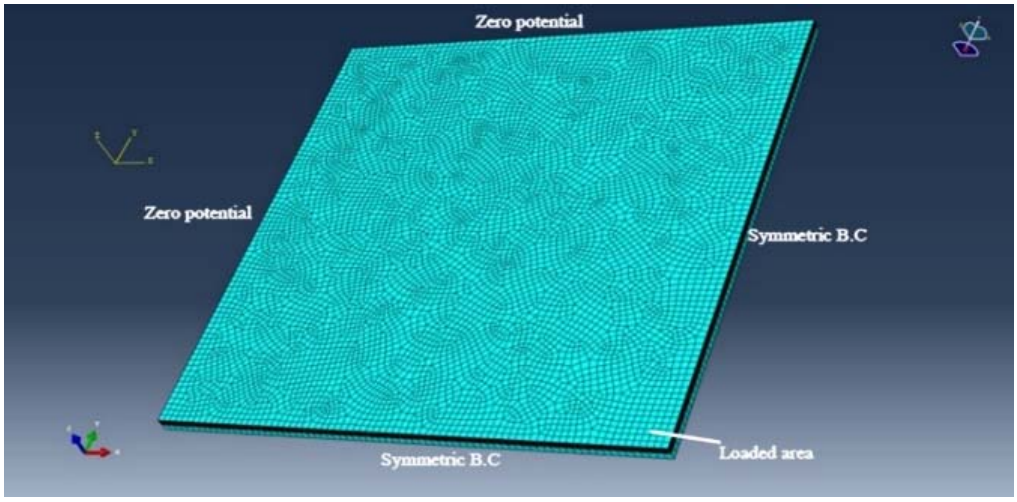

Fig. 15 Benchmark composite panel setup from impulse electrical current with applied boundary conditions

Each of the 16 top laminas is meshed with 7280 DC3D8 elements of type linear hexahedral, while the bottom 16 laminas are meshed as one part with average material properties, Total number of elements is 5776 DC3D8 of type linear hexahedral. Applying the electric current density load at the panel center leads to increase in temperature profile.

C. Results and Discussion

Coupled thermal/electrical FE analysis using temperature dependent material properties is used to simulate lighting strike on composite panel. Ablation mechanism for composite materials is simulated by defining ablation latent heat, and gas thermal/electrical properties conductivity. The laminate is damaged up to the 3th layer (0.441 mm), as shown in Fig. 18.

Experimental results, in Fig. 17 [7], show that recession is up to 0.4 mm, which agrees with the current results. The recession is mainly due to epoxy decomposition, which leaves a mix of fibers and carbon. The results Jennings and Hardwick [7] are very interesting because the theoretical results are compared with the experimental ones. The calculation domain used by Jennings and Hardwick is represented in Fig. 16: it only contains an anode of 2-mm height and 40-mm radius. The grid used includes 40 cells of 1 mm in the radial direction and 32 cells of 0.0625 mm in the axial direction.

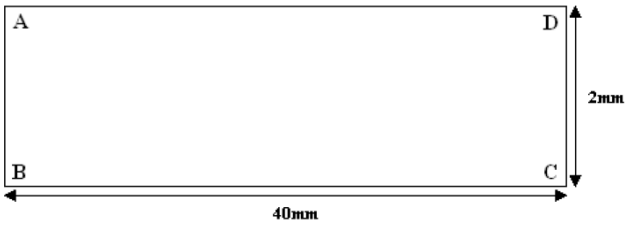

Fig. 16 Geometry used by Jennings and Hardwick [7]

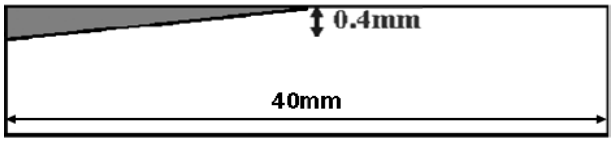

Fig. 17 Material degradation experimentally obtained by Jennings and Hardwick [7]

The results in terms of temperature field, or more exactly, in terms of material degradation, are represented in Figs. 19-22 at t = 0.5 s. It can be seen that the field given by the model differs from the experimental one in terms of degradation.

Differences are visible in both the depth of the degraded zone and its radius. This first part enabled us to compare the fields resulting from the developments set up in composite material with the literature. Good agreement was found with the experimental results given by Jennings and Hardwick [7] in terms of material degradation.

The temperature profile of the top layer is shown in Fig. 19. The dissipated electric energy is higher far from center. This is due to the lower electric conductivity along the depth direction and electric conductance between laminates. Thus, the electric current follows the easier path along the lamina fiber directions (top layer is 45° lamina). The maximum temperature achieved is 12106 °C, and the decomposition is defined in the range 0 to 1, while 0 represents virgin material and 1 represent fully decomposed and the material properties are switched to a mix of char and carbon fibers.

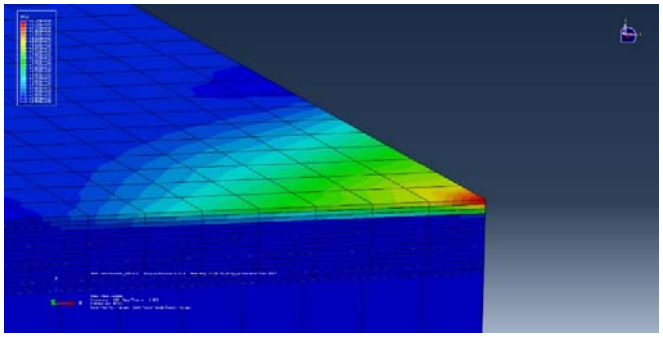

Fig. 18 Decomposed laminate layout

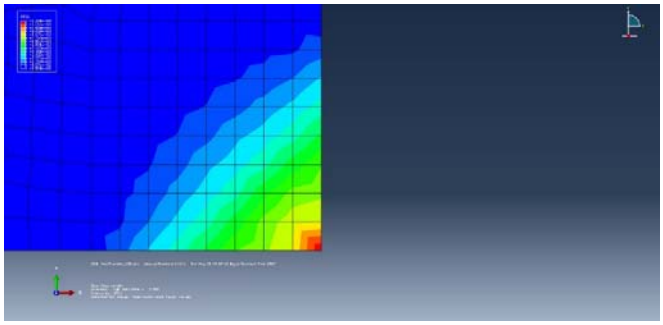

Fig. 19 Top lamina temperature profile

The heat energy coming from dissipated electric energy is transferred along the 45° fibers directions. Assuming that the damage threshold is defined by the area of decomposition degree higher than 0.3, the damage area is of 8.7 x 8.7 mm size, thus the epoxy is fully decomposed, and the lamina is ablated.

The lighting current strikes the top layer, which decomposes with time, then its electrical/thermal material properties are switched to a mix between char and fibers. Char has higher electric conductivity, which conducts better in the depth direction. So, the electric current reaches the next layer with 0° degree fibers. The next lamina to the top layer conducts electric charge in the fibers direction and conducts thermal heat from the top lamina, which accelerates the decomposition along the 0° direction and produces the following results.

In Fig. 19, the polymer degradation and fiber removal regions extend to the second ply below the surface. The shape of the decomposed region is elongated in the direction along the fibers since they provide easier conductive paths.

Temperature profile in the 2nd, 3rd, and 4th laminas are shown in Figs. 20-22. The maximum temperature is 9200 °C, 6600 °C, and 604 °C, respectively. Damage size is approximately 6.2 x 7.5 mm in 2nd lamina, and 3.75 x 3.75 mm in the 3rd lamina. The damage area is function of thermal conductivity of each lamina and thermal conductance between adjacent laminates.

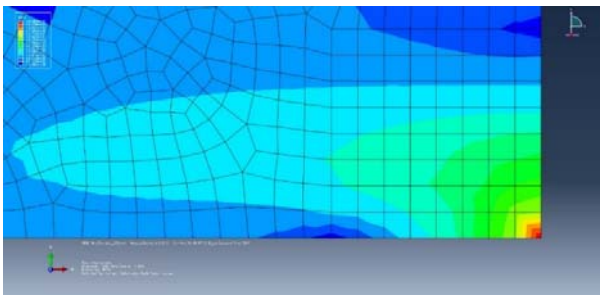

Fig. 20 Temperature profile for 2nd layer

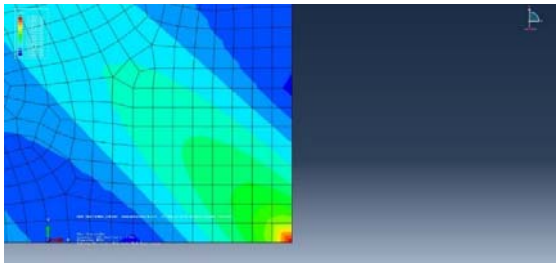

Fig. 21 Temperature profile for 3rd layer

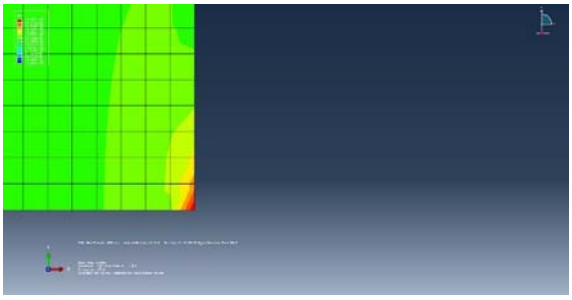

Fig. 22 Temperature profile for 4th layer

As a result, the material is decomposed, it behaves with char thermal/electrical properties until it is ablated (if temperature > 3316 °C). Char has higher specific heat, and convection boundary condition to air does not cool it quickly.

Including char material properties to model composite after decomposition and gas material properties to model composite after ablation produces realistic results. Using higher electric conductivity along the depth direction is limited only for the elements under electric current load to simulate the shift of the conducting electric channel to the next layer. The artificial

electric conductivity is not used for the rest of the model. Thus, the plasma current model captured the complex multiphysics of the lighting strike on composite panel by using electric current density load, using temperature dependent material properties, and including char and gas material properties to simulate after decomposition and ablation, respectively.

Results indicated that, during lightning strike, composite laminate damage behaviour propagates quickly at the initial phase of lightning strike event, and then becomes slowly, because of the act of resistive heating generated by electricity conduction in-plane of the lamina and heat transfers between connected laminas, and then propagates directionally created damage of each lamina; with the increase of time versus applied current density and waveform parameters, damage of the composite laminates will be increased as it is confirmed in a previous work in [4]. Next, a protection layer of copper mesh is applied, and simulation results are discussed.

VI. Lightning Strike Protection (LSP)

In order to protect composite material, in addition to the zoning procedure, several protections have been designed to help maintaining the structural integrity of impacted parts [20]. These protections aim to protect and prevent composite parts from serious damage. Ideally, a good lightning metal protection should have: a good conductivity in order to evacuate lightning currents, a low temperature of fusion and vaporization, light weight in order to minimize the additional weight due to the lightning protection, a good behaviour against corrosion (air, rain…), good mechanical properties, easy to maintain and repair, easy to shape for complex structure elements shape, and low cost.

The protection has to absorb the impact energy in order to limit the mechanical and thermal effects on the laminate. It also has to be a good conductor to conduct the received current and its associated energy out of the structure. Unfortunately, these protections are not always sufficient and the systematic adding of paint (dielectric material) by aeronautical companies decreases the effects of the protection. Moreover, these protections are to cover the whole structure and it results in an additional weight that reduces the gain made up by using composite materials. The most common used protections are the following [21].

In this section, we propose an improved technique to study the lighting strike effects on composite panel with protection system. A user material subroutine is used to model the complex physical behavior of the protection system. Thermal performance of composite laminate is different from lighting strike protection system. The composite material thermal performance is characterized by resistive heating, decomposition, and ablation. Meanwhile, the protection system thermal performance is characterized by resistive heating, melting, evaporation, and then explosive boiling.

Copper thermal performance is simulated using ABAQUS user material subroutine UMATHT, which is used to define the thermal constitutive behavior of the material as well as internal heat generation during heat transfer processes. It must define the internal energy per unit mass and its variation with respect to temperature and to spatial gradients of temperature, and the heat flux vector and its variation with respect to temperature and to gradients of temperature.

A. FE Model

The commercial code ABAQUS, version 6.12.1, was used to simulate material status after decomposition, gas material properties to simulate material ablation status, and modeling the complex physics of protection systems using UMATH material subroutine. Simulation of the protection system included modeling melting, evaporation, and ablation, while interacting with the composite panel through temperature dependent thermal conductance property.

Metal mesh and special types of conducting paint are used for lightning strike protection of composite panels. For instance, copper mesh is used for lightening protection and it has melting temperature T_m of 1083 ^{o}C, boiling temperature T_b of 2800 ^{o}C, and critical temperature T_c of 8000 ^{o}C.

Copper mesh is used in this work as candidate for the lighting strike protection system as shown in Fig. 23. Copper mesh thickness is 0.05 mm and it covers the whole aircraft skin area. However, the modeling techniques can be applied to any different protection systems, such as aluminum mesh or paint. The function of the copper mesh is to conduct the lighting strike electric charge quickly and protect the underneath composite material from damage. The copper mesh will cover 100% of the aircraft wing area, electric charge always chooses the easy path.

Under the lighting strike electric conditions, the copper will heat up, according to its specific heat property until it reaches its melting temperature point ($1083^{o}C$) and it consumes the heat of fusion (2.05 x10^5 J/kg). Then, the copper will keep heating up until it reaches its boiling point ($2567^{o}C$) and starts consuming its heat of evaporation (4.8x10^6 J/kg) as it evaporates. Heating up and evaporation of copper (protection system) is stopped by the following two mechanisms; total ablation of the copper mesh or explosive boiling of the copper mesh as it reached its critical temperature ($8000^{o}C$).

The damage effect of explosive boiling is not modeled in this work and the critical temperature can be used as a threshold for design of lightning strike protection systems. Copper thermal/electrical properties are defined from [4]. Real geometry of the copper mesh is used over the entire panel as shown in Fig. 24. Copper mesh is meshed with 304,276 DC3D8E elements. Each of the 16 top laminas is meshed with 7280 DC3D8 elements of type linear hexahedral, while the bottom 16 laminas are meshed as one part with average material properties. Total number of elements is 5776 DC3D8 of type linear hexahedral. Applying the electric current density load at the panel center leads to increase in temperature profile in Fig. 25.

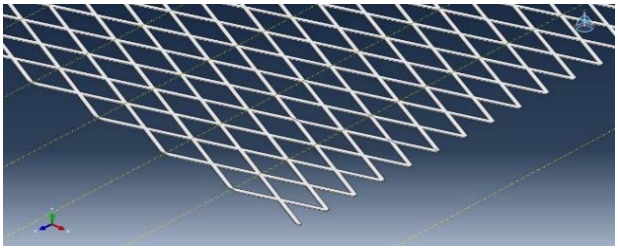

Fig. 23 Copper mesh panel used in the model

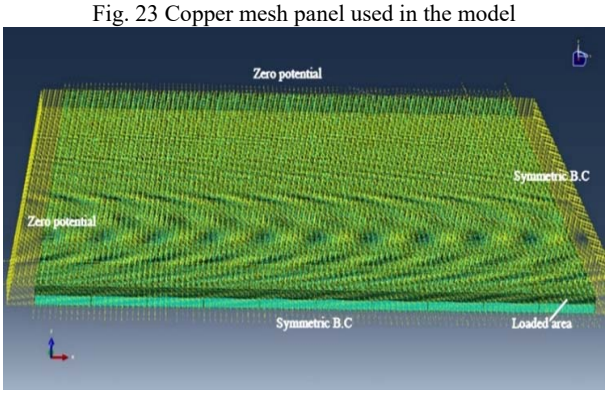

Fig. 24 Benchmark protected meshed composite panel setup from impulse electrical current with applied boundary conditions

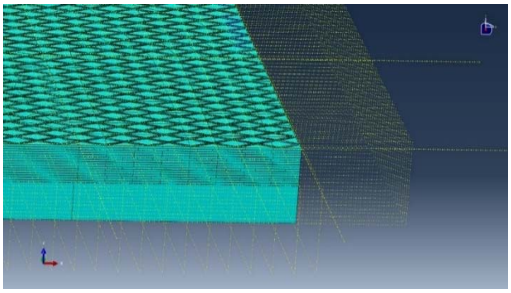

Fig. 25 Protected meshed composite panel at the panel center

B. Glass/Epoxy Lamina (GF)

It is a general practice of the aerospace companies to include a glass/epoxy lamina in between the copper mesh and the composite panel. Two advantages can be achieved by the inclusion of glass/epoxy lamina. One advantage is to act as a thermal insulation layer between the copper mesh and the composite panel. Second advantage is that the glass/epoxy has two reaction heats under high thermal environment. One reaction heat of value 239 kJ/kg is consumed during decomposition of epoxy and another reaction heat between carbon and silica consumes 2093 kJ/kg. E-Glass fiber/epoxy thermal and electrical material properties are given in Table III. These data are provided subject to AZoM.com's terms and conditions. Data are reproduced with permission of Granta Design Limited. Besides, corrosion of metals is of particular concern when in contact with the composites. There is a potential for corrosion due to dissimilar metals contacts. So that, the following is applied to composites that are in contact with metal structure: a fiberglass barrier ply covers the entire faying surface of the composite with thickness 0.147 mm. No splices are allowed in the barrier ply. This design philosophy has proven to be effective. Thus far, there have been no service reports related to dissimilar metals corrosion. It should be noted that commercial LSP systems often possess a glass fiber isolation ply which is sometimes used to prevent galvanic corrosion that occurs between carbon fiber substrate and the metallics in the LSP system (especially those that possess a dissimilar galvanic potential relative to that of carbon).

TABLE III
E-GLASS FIBER/EPOXY THERMAL AND ELECTRICAL MATERIAL PROPERTIES

Material:	E-Glass Fiber	
Composition:	54%SiO_2-15%Al_2O_3-12%CaO	
Property	Mini. Value	Maxi. Value
Atomic Volume (Average) (m^3/kmol)	0.0088	0.009
Density (Mg/m^3)	2.55	2.6
Poisson's Ratio	0.21	0.23
Young's Modulus (GPa)	72	85
Glass Temperature (K) (T_g)	820	850
Specific heat (J/kg.K)	800	805
Thermal conductivity (W/m.K)	1.2	1.35
Thermal Expansion (10^{-6} /K)	4.9	5.1
Breakdown Potential (MV/m)	15	20
Resistivity (10^{-8} ohm.m)	1 x 10^{22}	1 x 10^{23}

Finally, glass fiber layer is meshed with 5776 DC3D8 elements of type linear hexahedral. The model structure layup consists of copper mesh (ECF), FG (glass/ epoxy), and finally our composite laminates.

C. Results and Discussion

Figs. 26 and 27 show temperature profile to investigate the behavior of the copper mesh and the glass/epoxy laminas under lighting strike. We found that there is no damage to the composite material. The ablation is not fast enough, which allows the copper to heat up to its critical temperature (8000 ^oC). This means the copper in the area of the lighting strike heats up to the explosive boiling state and may cause more damage to the composite panel. Effect of explosive boiling damage is not modeled, assuming that it is a critical point that has to be evaded in designing a protection system. Thickness of the protection system is small compared to the total thickness of the full composite panel, thus magnetic forces effect can be ignored.

The function of the protecting copper mesh is to conduct rapidly the electric charge away from the lighting strike zone, thus reducing the damage applied on the composite panel. Copper conducts electric charge which heats it up to the melting point (1083 ^oC), then up to the evaporation temperature (2567 ^oC), where it starts ablation. The damage mechanism for the composite material is thus controlled by the conducting heat with the copper, which is defined by the thermal conductance between copper mesh and composite material.

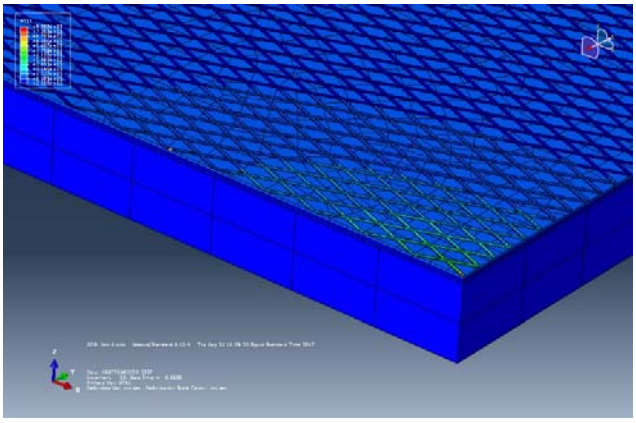

Fig. 26 Temperature profile for the composite laminate including the copper mesh metal (ECF) and GF

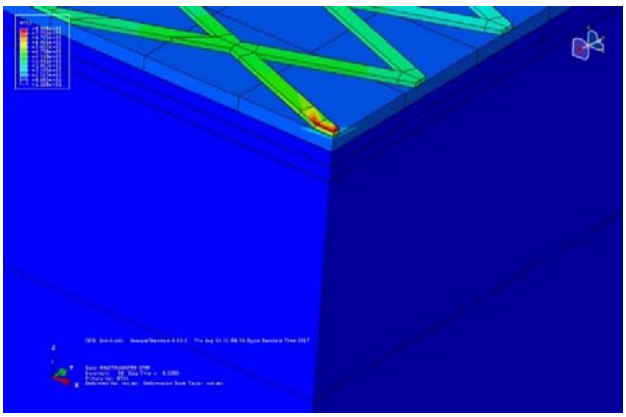

Fig. 27 Temperature profile for the composite laminate including the copper mesh metal (ECF) and GF at the panel center

VII. Conclusion

This paper presents state of the art numerical procedures to investigate the effects of lightning strike on composite laminate without/with protection (LSP) systems. Thus, a coupled thermal-electrical finite element analysis (FEA) procedure is proposed to enable the investigation of the design variables that control lightning strike damage in graphite/ epoxy composites. The major contribution of this study is the formulation and verification of temperature dependent material properties, a key attribute not considered within the previous literature. The proposed procedure is applied to a test specimen and the results are verified against published experimental data, illustrating the accuracy and computational cost of lightning strike simulation and the requirement for temperature dependent material properties. The procedure is then applied to a practical LSP system, and the simulation results are used to further understand and quantify the physical behavior that minimizes material damage. Initially, the 2D MHD numerical approach of lightning plasma is used to simulate waveform-C event on a composite structure. The multiphysics model simulates the lightning strike channel effect to estimate electric current, pressure, and heat fluxes are more accurately determined at the anode (composite structure) and results are validated using published experimental data. The order of estimated temperature (of the order of 40,000 K) and pressure (of the order of 0.1-0.2 MPa) suggests that the waveform – C damage is mainly due to thermoelectric effect, while pressure effect is minimum. The MHD provides more accurate input parameters at the anode surface. Then, on the level of the interaction between the plasma arc and composite laminate, ABAQUS 3D coupled thermal – electric model is then used to estimate the temperature fields, thus the composite material damage due to the joule heat effect for duration 0.5 s.

Finally, improved lightning strike's thermal protection system (LSP) is necessary to reduce running maintenance cost of aircraft composite structures. In this part, we added both of copper mesh protection panel and glass/epoxy layers to composite laminate, Copper conducts rapidly the electric charge away from the lighting strike zone and the glass fiber acts as a thermal insulation layer between the copper mesh and the composite panel. Thus, there is no damage in the composite model. The work in this paper is the first phase of a long research project to investigate the lighting strike multiphysics problem on composite structures. The MHD model needs improvements to model waveform – A, B, and D, principally due to the heat transfer FE size constraint, which is limited by the time – step size. Additionally, investigating using the finite volume approach instead of the FE one is more stable for CFD models. We may ppgrade the MHD model to simulate the plasma multicomponent (electrons, ions) diffusion and chemical reactions using CENTERA to understand in more details the plasma channel interaction with the TPS surface. In this case, the MHD plasma model will be more realistic to investigate the design parameters of the ionized plasma channel and study its interaction with the aircraft composite structure.

References

[1] EUROCAE ED-84, 1997, Aircraft Lightning Environment and Related Test Waveform Standard.
[2] SAE Committee report: ARP-5412, July 1999, Aircraft Lightning Environment and Related Test Waveforms Standard.
[3] Hirano Y, Yoshimura A, Ogasawara T., 2010, Coupled thermal-electrical analysis for carbon/epoxy composites exposed to simulated lightning current, Composite Part A, 41, p.973-981.
[4] G. Abdelal and A. Murphy, 2014, Nonlinear numerical modelling of lightning strike effect on composite panels with temperature dependent material properties, Composite Structures, 109, 268-278.
[5] L. Chemartin, P. Lalande, B. Peyrou, A. Chazottes, P.Q. Elias, 2012, Direct Effects of Lightning on Aircraft Structure: Analysis of the Thermal, Electrical and Mechanical Constraints, Journal of Aerospace Lab, Issue 5.
[6] J.-P. Parmantier, 2012, Indirect Effects of Lightning on Aircraft and Rotorcraft, Journal Aerospace-Lab, Lightning Hazards to Aircraft and Launchers, Issue 5, pp.20–24.
[7] Jennings N. and Hardwick C. J., 1992, A computational approach to predicting the extent of arc root damage in CFC panels, 15th Int. Aerospace and Ground Conf. on Lightning and Static Electricity (Atlantic City) pp 41.1–41.8.
[8] Y. Wang, O.I. Zhupanska, 2015, Lightning strike thermal damage model for glass fiber reinforced polymer matrix composites and its application to wind turbine blades, Composite Structures 132, 1182–1191.
[9] F. Tholin, L. Chemartin, P. Lalande, 2015, Numerical investigation of the interaction of a lightning and an aeronautic skin during the pulsed arc phase, International Conference on Lightning and Static Electricity (ICOLSE), Toulouse.

[10] Boulos M I, Fauchais P and Pfender E 1994 Thermal plasma, Fundamentals and applications vol 1 (New York: Plenum) ISBN 0306446073.
[11] Naghizadeh-Kashani Y 1999 Calcul du transfert radiatif dans un plasma d'air Thesis 3488, Universit´e Paul Sabatier, Toulouse.
[12] M. Tanaka and JJ. Lowke. Predictions of weld pool profiles using plasma physics. Journal of Physics D-Applied Physics, 40:R1{R23, 2007.
[13] JJ. Lowke, R. Morrow, and J. Haidar. A simplified unified theory of arcs and their electrodes. Journal of Physics D: Applied Physics, 30(14):2033, 1997.
[14] M. Tanaka, H. Terasaki, M. Ushio, and JJ. Lowke. A unified numerical modeling of stationary tungsten-inert-gas welding process. Metallurgical and Materials Transactions A-Physical Metallurgy and Materials Science, 33:2043{2052, 2002.
[15] Larsson A, Lalande P, Bondiou-Clergerie A and Delannoy A2000 The lightning swept stroke along an aircraft in flight. Part I: thermodynamic and electric properties of lightning arc channels J. Phys. D: Appl. Phys. 33 1866–75.
[16] Larsson A, Lalande P, Bondiou-Clergerie A and Delannoy A2000 The lightning swept stroke along an aircraft in flight. Part II: numerical simulations of the complete process J. Phys. D: Appl. Phys. 33 1876–83
[17] Uhlig F 1998 Contribution `a l'´etude des effets directs du foudroiement sur les mat´eriaux structuraux constituant un a´eronef Thesis Universit´e de Paris.
[18] Hsu K C, Etemadi K and Pfender E 1983 Study of the free-burning high-intensity argon arc J. Appl. Phys. 54 1293–301.
[19] O.H. Nestor, "Heat intensity and current density distributions at the anode of high current, inert gas arcs", Appl. Phys. 33, 5 1638-1648, 1962.
[20] Fischer F A, Plumer J A and Perala R A 1977 Lightning protection of aircraft NASA Reference Publication 1008 (NASA Lewis Research Center.
[21] M. Gagné, D. Therriault, 2014, Lightning strike protection of composites, Progress in Aerospace Sciences 64, 1–16.